JOURNAL OF BACTERIOLOGY, Mar. 2011, p. 1131–1141 Vol. 193, No. 5
0021-9193/11/$12.00 doi:10.1128/JB.01153-10

In Vivo Recognition of the *fecA3* Target Promoter by *Helicobacter pylori* NikR▽

Simona Romagnoli, Francesca Agriesti, and Vincenzo Scarlato*

Department of Biology, University of Bologna, Bologna, Italy

Received 28 September 2010/Accepted 22 December 2010

In *Helicobacter pylori*, the transcriptional regulator *Hp*NikR represses transcription of the *fecA3* gene by binding to two adjacent operators spanning a region of almost 80 nucleotides along the *fecA3* promoter in a nickel-dependent manner. By employing hydroxyl radical footprinting, we mapped the protected nucleotides within each operator. Three short sequences rich in A and T nucleotides were identified within each operator, comprising just 24 bases for both operators, with 4 or 5 protected bases interspaced by 4 to 7 free nucleotides, with no center of symmetry. Base substitutions at any site strongly reduced the affinity of *Hp*NikR for the operators and also affected the stability of the DNA-protein complex, when the promoter-regulator interaction was analyzed *in vitro*. The effect of these substitutions was remarkably different when transcription of the mutant promoters was analyzed *in vivo*. Base changes introduced at the farthest subsites impaired the *Hp*NikR-dependent repression, with the mutations closer to +1 completely abolishing the repression, the more distal one still allowing almost 50% of transcription, and the mutations in the middle being ineffective. The data presented here show that *Hp*NikR may first select its targets by identifying sequences within the previously defined consensus and subsequently establish base-specific contacts to firmly bind DNA. In particular, *Hp*NikR seems to interact in an asymmetric mode with the *fecA3* target to repress its transcription.

*Hp*NikR is a master regulator in *Helicobacter pylori*, directly up- and downregulating the expression of genes involved in nickel uptake, storage, and usage (12, 14, 15, 22, 40, 43), as well as iron homeostasis and acid response, and indirectly partaking in a global regulatory cascade governing virulence and pathogenicity (7, 10, 13, 21, 39). So far, direct binding to 8 target genes has been experimentally proven (12, 15, 22, 40, 43), leading to a general model of regulation where *Hp*NikR binding upstream of the promoter region recruits the RNA polymerase to the promoter and therefore activates transcription, whereas downstream binding to operators overlapping the −10 or −35 hexamer boxes represses transcription by a simple steric hindrance mechanism. Comparison of characterized *Hp*NikR DNA operators shows little identity of sequence (15, 20). An imperfect A- and T-rich palindrome was proposed as an *Hp*NikR consensus box by Delany et al. (15), and recently Stoof et al. (37) presented a revised similar consensus motif, based on the bioinformatics analysis of selected high-affinity target promoters. So far, the only study examining what specific base contacts *Hp*NikR made on a nickel-activated promoter (P_{ureA}) and a nickel-repressed promoter (P_{nixA}) revealed the prevalence of T and A nucleotides directly bound by *Hp*NikR within short sequences surrounding the putative consensus motif (5).

*Hp*NikR belongs to the RHH (ribbon-helix-helix) family of transcriptional regulators (8). This heterogeneous family is characterized by an N-terminal ribbon-helix-helix (βαα) DNA binding domain with a recognition antiparallel β sheet fitting the major groove of a DNA operator and the second α helix making contacts with the DNA phosphate backbone (33). As for *Escherichia coli* NikR (*Ec*NikR), polar interactions of the residues within the C-terminal metal binding domain, in addition to unspecific electrostatic contacts, contribute to stabilizing the binding to the operator (35). In contrast with other components of this large family of regulators, NikR is a dimer of dimers, folding as a stable tetramer both in the apo- and in the holo-form (34), with the binding of the physiological effector Ni^{2+}, increasing the affinity for the target promoter and stabilizing the interactions with the operator. The structural analysis of the *Ec*NikR protein revealed that the large C-terminal metal binding domain calls for an operator segment longer than the ones recognized by other regulators of the RHH family (11, 26, 27, 35). In *E. coli*, NikR is a repressor of the *nikABCDE* operon (9, 17), encoding the nickel-specific ABC transporter. The structure of the *Ec*NikR-*nik* complex (35) highlighted the presence of tandem binding sites arranged as inverted repeats separated by 16 nucleotides. These authors also observed that a static conformation of the protein would put the DNA binding domains too far apart to bind the half-sites on a linear DNA operator; therefore, the allosteric change induced by nickel binding to the regulator should promote mutual conformation adjustments, via the interdomain flexible linker, between the protein and the target DNA to allow a productive interaction.

In recent years, a great many studies have addressed the metal requirement of *Hp*NikR and the consequent activation inducing DNA binding (1, 2, 18, 19, 45). Because of the stoichiometric binding of nickel to *Hp*NikR, the different affinities to diverse promoters of *Hp*NikR respond to distinct physiological needs, establishing a rank of interactions with high- and low-affinity *Hp*NikR-regulated promoters (20). In addition, the broad variation of pH encountered by *H. pylori* during the invasion of the host tissues (31) puts *Hp*NikR and the nickel

* Corresponding author. Mailing address: Department of Biology, University of Bologna, Via Selmi, 3, 40126 Bologna, Italy. Phone: 39 051 209 4204. Fax: 39 051 209 4286. E-mail: vincenzo.scarlato@unibo.it.

▽ Published ahead of print on 7 January 2011.

enzymes (urease and hydrogenase) in competition for Ni^{2+} ions (4), underlining the importance of balancing intracellular activities, and also raises the possibility of activation of *Hp*NikR DNA binding activity upon acidic shifts (24). Finally, the N-terminal arm nine residues, unique to *Hp*NikR, exert an inhibitory role preventing nonspecific DNA binding but also directly interact with specific target promoters, in the presence of additional cations (5).

In spite of all these functional details, how *Hp*NikR binds to DNA *in vivo* is not well understood. In this study, we characterized the interactions that *Hp*NikR makes along the *fecA3* promoter *in vitro* and assayed transcription *in vivo*. By employing hydroxyl radical footprinting, we mapped the bases protected by *Hp*NikR within P_{fecA3}, as well as within the P_{nikR} and P_{exbB} *Hp*NikR-regulated promoters. Notably, the sequences of protected bases among the promoters were not conserved and map in proximity to the previously defined consensus motif (15, 37), suggesting that *Hp*NikR may first identify its targets, possibly recognizing the consensus sequence, and subsequently directly interact with bases flanking or partially overlapping the consensus.

MATERIALS AND METHODS

Bacterial strains and growth conditions. *H. pylori* G27 was the parental strain used in this study (Table 1). Wild-type (44) and Δ*nikR*::Km (29) strains containing an extralocus transcriptional fusion of the wild-type and mutant promoters were constructed as described below. The strains were streaked from −80°C glycerol stocks on brucella agar plates with 5% fetal calf serum (Oxoid) and Dent's or Skirrow's antibiotic supplement and grown at 37°C under microaerophilic conditions (9% CO_2, 91% air atmosphere, 95% humidity) in a water-jacketed thermal incubator. Liquid cultures were grown in a modified brucella broth supplemented with 5% fetal calf serum (Oxoid) and Dent's or Skirrow's antibiotic supplement at 37°C under constant agitation (125 rpm). To measure the nickel-dependent transcriptional repression, master cultures (25 ml) of the strain under examination were grown to mid-log phase (optical density at 600 nm [OD_{600}], 0.5 to 0.6), divided into two equal-volume (10-ml) subcultures, and treated for 15 min with freshly made 1 mM $NiSO_4$ before RNA extraction. *Escherichia coli* strains DH5α and BL21(DE3) were grown in Luria-Bertani broth. Ampicillin (100 μg/ml), kanamycin (25 μg/ml), and chloramphenicol (30 μg/ml) were added when required.

DNA manipulation and mutagenesis of the promoter region of *fecA3*. Standard molecular biology techniques were utilized for DNA manipulations (32). All restriction and modification enzymes (New England BioLabs) and PCR cleanup and gel extraction DNA purification kits (Qiagen) were used according to the manufacturers' instructions. A SmaI site was introduced within the *fecA3* operators to change the nucleotides contacted by *Hp*NikR and, therefore, create mutant *fecA3* promoters. Six different full-length constructs were generated by PCR, using the primers listed in Table 2 and by following a recently described strategy (12). In detail, the primer pair A3Fnew-A3.12 and A3Rnew-A3.11 was used to generate pA3.1; the primer pair A3Fnew-A3.14 and A3Rnew-A3.13 was used to generate pA3.15; the primer pair A3Fnew-A3.16 and A3Rnew-A3.15 was used to generate pA3.16; the primer pair A3Fnew-A3.18 and A3Rnew-A3.17 was used to generate pA3.17; the primer pair A3Fnew-A3.20 and A3Rnew-A3.19 was used to generate pA3.19; the primer pair A3Fnew-A3.22 and A3Rnew-A3.21 was used to generate pA3.21; pGemT-P_{fecA3} (12) was used as the template. The regions of interest were PCR amplified, subcloned in pBluescript SK (Stratagene), and subsequently ligated via the SmaI site to generate the desired plasmid. All mutations were confirmed by sequence analysis.

Construction of *lacZ* transcriptional fusions and integration in the *vacA* locus of *H. pylori*. The wild-type and mutant *fecA3* promoters were cloned via the restriction sites BamHI and EcoRI into pBluescript SK so as to have transcriptional fusions in frame with the *lacZ* 3′ region occurring on the vector. These constructs were recovered by PvuII-BamHI double digest, blunted, and cloned into the pVac::Km vector by exploiting a HincII site, as previously described (12). When needed, a chloramphenicol resistance cassette was recovered by an XhoI-XbaI double digest from plasmid pBS-CAT (41). The resulting fragment was blunted and ligated into a filled-in XbaI site present on the pVac::Km vector. The resulting extralocus copy of the promoter was inserted in the *vacA* locus on the chromosome of *H. pylori* by homologous recombination; the transcriptional fusions were transformed in *H. pylori* wild-type and Δ*nikR*::Km strains. Positive colonies were selected on agar plates by antibiotic resistance. The integrations were confirmed by PCR amplification with primers A3Z1 and A3F.new.

RNA isolation and primer extension analyses. Total RNA was extracted by a hot-phenol procedure as described previously (12). Primer extension analyses were performed on 15 μg of total RNA with 5 pmol of 5′-end-labeled A3Z1 primer and avian myeloblastosis virus (AMV) reverse transcriptase (Promega). The transcription start site of the corresponding cloned promoter region was mapped in a sequencing reaction using *Taq* polymerase. Following image acquisition by a Storm PhosphorImager (Molecular Dynamics), the extension products were quantified by ImageQuant software.

Overexpression and purification of recombinant His_6-*Hp*NikR. Recombinant His_6-*Hp*NikR (15) was overexpressed and purified under native conditions. The N-terminal histidine tag was removed by thrombin (Amersham GE Healthcare) cutting; untagged *Hp*NikR protein was stored in aliquots in phosphate-buffered saline (PBS) at −80°C (12). Prior to the DNA binding experiments, *Hp*NikR was dialyzed overnight against the assay reaction buffer.

Probe preparation and hydroxyl radical footprinting. The vectors containing the wild-type and mutant forms of the *fecA3* promoter and the promoters of the divergently transcribed *nikR* and *exbB* genes were linearized with EcoRI (or BamHI), dephosphorylated with calf intestinal phosphatase, and labeled at the 5′ end with [γ-^{32}P]ATP (5,000 Ci/mmol; Perkin-Elmer) using T4 polynucleotide kinase. The labeled DNA probe was further digested with BamHI (or EcoRI), and the end-labeled probes were recovered as previously described (12). The binding reactions between approximately 20 fmol of labeled probe and increasing concentrations of *Hp*NikR (expressed per NikR tetramer) were carried out in OH footprinting buffer (50 mM Tris-Cl, pH 7.85, 50 mM KCl, 10 mM $MgCl_2$, 0.01% Igepal) in the presence of an excess of $NiSO_4$ (100 μM) at room temperature for 15 min using 1 μg of salmon sperm DNA (Invitrogen) as nonspecific competitor. Two microliters of 0.1 M dithiothreitol (DTT), 2 μl of freshly made 125 mM $[(NH_4)_2Fe(SO_4)_2 \cdot 6H_2O]$/250 mM EDTA mix, and 2 μl of 1% H_2O_2 were simultaneously added to a final volume of 30 μl, incubated for 2 min, immediately quenched with 25 μl of stop buffer (4% glycerol, 0.6 M sodium acetate [NaOAc], pH 5.2, 0.1 μg of salmon sperm DNA), and treated as described in reference 46. Heat-denatured samples were separated on 8 M urea-8.4% polyacrylamide sequencing gels and autoradiographed. A modified G+A sequencing ladder protocol (25) was utilized to map the protected nucleotides.

DNA electrophoretic mobility shift assay. A DNA gel retardation assay was performed on the wild-type and mutant full-length *fecA3* promoters, previously purified from the gel as described for the footprinting experiments. The binding reaction was carried out for 15 min in 20 mM HEPES-OH (pH 7.85), 50 mM KCl, 10% glycerol, 0.02% Igepal CA-630, 0.1 mM DTT (12, 45), with 200 ng of salmon sperm DNA as nonspecific competitor. Twenty femtomoles of radiolabeled target DNA and increasing concentrations of *Hp*NikR were used in a final volume of 15 μl in the presence of 100 μM $NiSO_4$. Reaction mixtures were resolved onto a native gel (4% polyacrylamide [19:1], 20 mM MOPS [morpholinepropanesulfonic acid], 5 mM NaOAc, pH 7.0), prerun at 50 V for 30 min prior to loading, and then run at 170 V for 2 h at room temperature. A Storm PhosphorImager (Molecular Dynamics) was utilized to acquire the gels; the band shifts were quantified by ImageQuant software.

RESULTS

Identification of nucleotides directly contacted by *Hp*NikR. In a previous study (12), we showed that *Hp*NikR protected an extended region within the *fecA3* promoter comprising two operators, OP-I at high affinity and OP-II at low affinity, both of approximately 40 bp and spanning nucleotides −46 to +31 with respect to the transcription start site (Fig. 1A). To identify the nucleotide sequence contacted by *Hp*NikR, we carried out hydroxyl radical footprinting on both DNA strands of the *fecA3* promoter in the presence of increasing concentrations of *Hp*NikR (Fig. 1B and C). Three discrete and distinct regions of protection were observed within both operators, with the subsites of OP-I detected at 49 nM (Fig. 1B, lane 3) and the ones of the OP-II detected at 112.7 nM (Fig. 1C, lane 4), as ex-

TABLE 1. Strains and plasmids used in this study

Strain or plasmid	Genotype	Reference or source
Bacterial strains		
E. coli		
DH5α	*supE44* Δ*lacU169* (ϕ80 *lacZ*ΔM15) *hsdR17 recA1 endA1 gyrA96 thi-1 relA1*β	23
BL21(DE3)	*hsdS gal* (λc*Its*857 *ind1 Sam7 nin5 lacUV5-T7 gene 1*)	38
H. pylori		
G27	Clinical isolate; wild type	44
Δ*nikR*::Km strain	G27 derivative with *nikR* partially deleted; Km^r	29
G27vac::PA3 *lacZ* strain	G27 derivative containing the wild-type P_{fecA3} promoter-*lacZ* fusion in the *vacA* locus; Km^r	This study
G27vac::PA3.1 *lacZ* strain	G27 derivative containing the OP-I mutant $P_{fecA3.1}$-*lacZ* fusion in the *vacA* locus; Km^r	This study
G27vac::PA3.15 *lacZ* strain	G27 derivative containing the OP-I mutant $P_{fecA3.15}$-*lacZ* fusion in the *vacA* locus; Km^r	This study
G27vac::PA3.16 *lacZ* strain	G27 derivative containing the OP-I mutant $P_{fecA3.16}$-*lacZ* fusion in the *vacA* locus; Km^r	This study
G27vac::PA3.17 *lacZ* strain	G27 derivative containing the OP-II mutant $P_{fecA3.17}$-*lacZ* fusion in the *vacA* locus; Km^r	This study
G27vac::PA3.19 *lacZ* strain	G27 derivative containing the OP-II mutant $P_{fecA3.19}$-*lacZ* fusion in the *vacA* locus; Km^r	This study
G27vac::PA3.21 *lacZ* strain	G27 derivative containing the OP-II mutant $P_{fecA3.21}$-*lacZ* fusion in the *vacA* locus; Km^r	This study
Δ*nikR*::Km vac::PA3.1 *lacZ* strain	Δ*nikR* strain derivative containing the OP-I mutant $P_{fecA3.1}$-*lacZ* fusion in the *vacA* locus; Km^r Cp^r	This study
Δ*nikR*::Km vac::PA3.15 *lacZ* strain	Δ*nikR* strain derivative containing the OP-I mutant $P_{fecA3.15}$-*lacZ* fusion in the *vacA* locus; Km^r Cp^r	This study
Δ*nikR*::Km vac::PA3.16 *lacZ* strain	Δ*nikR* strain derivative containing the OP-I mutant $P_{fecA3.16}$-*lacZ* fusion in the *vacA* locus; Km^r Cp^r	This study
Plasmids		
pBluescript SK (pBS)	General cloning vector; Amp^r	Stratagene
pA3	pBluescript derivative containing the wild-type fragment of the *fecA3* promoter region, amplified by PCR with primers A3Fnew and A3Rnew	12
pA3.1	pA3 derivative containing 265 bp of *fecA3* promoter region with a SmaI site in OP-I generated by PCR amplification of the wild-type construct with primers A3Fnew-A3.12 and A3Rnew-A3.11 and subsequent ligation at the SmaI site	This study
pA3.15	pA3 derivative containing 265 bp of *fecA3* promoter region with a SmaI site in OP-I generated by PCR amplification of the wild-type construct with primers A3Fnew-A3.14 and A3Rnew-A3.13 and subsequent ligation at the SmaI site	This study
pA3.16	pA3 derivative containing 265 bp of *fecA3* promoter region with a SmaI site in OP-I generated by PCR amplification of the wild-type construct with primers A3Fnew-A3.16 and A3Rnew-A3.15 and subsequent ligation at the SmaI site	This study
pA3.17	pA3 derivative containing 265 bp of *fecA3* promoter region with a SmaI site in OP-II generated by PCR amplification of the wild-type construct with primers A3Fnew-A3.18 and A3Rnew-A3.17 and subsequent ligation at the SmaI site	This study
pA3.19	pA3 derivative containing 265 bp of *fecA3* promoter region with a SmaI site in OP-II generated by PCR amplification of the wild-type construct with primers A3Fnew-A3.20 and A3Rnew-A3.19 and subsequent ligation at the SmaI site	This study
pA3.21	pA3 derivative containing 265 bp of *fecA3* promoter region with a SmaI site in the OP-II generated by PCR amplification of the wild-type construct with primers A3Fnew-A3.22 and A3Rnew-A3.21 and subsequent ligation at the SmaI site	This study
pBS-CAT	pBluescript derivative containing the chloramphenicol resistance cassette from *Campylobacter coli*; Amp^r Cp^r	41
pVac::Km	pGemZ derivative containing a kanamycin cassette	16
pVac::PA3*lacZ*	pVac::Km derivative containing the transcriptional fusion P_{fecA3}::*lacZ*; Km^r	This study
pVac::PA3.1*lacZ*	pVac::Km derivative containing the transcriptional fusion $P_{fecA3.1}$::*lacZ*; Km^r Cp^r	This study
pVac::PA3.15*lacZ*	pVac::Km derivative containing the transcriptional fusion $P_{fecA3.15}$::*lacZ*; Km^r Cp^r	This study
pVac::PA3.16*lacZ*	pVac::Km derivative containing the transcriptional fusion $P_{fecA3.16}$::*lacZ*; Km^r Cp^r	This study
pVac::PA3.17*lacZ*	pVac::Km derivative containing the transcriptional fusion $P_{fecA3.17}$::*lacZ*; Km^r	This study
pVac::PA3.19*lacZ*	pVac::Km derivative containing the transcriptional fusion $P_{fecA3.19}$::*lacZ*; Km^r	This study
pVac::PA3.21*lacZ*	pVac::Km derivative containing the transcriptional fusion $P_{fecA3.21}$::*lacZ*; Km^r	This study
pNKTB	pGemT derivative containing the *nikR-exbB* intergenic region; Amp^r	15
pET15b	IPTG[a]-inducible, N-terminal His_6-tagged recombinant protein overexpression vector; Amp^r	Novagen
pET15b-*nikR*	pET15b derivative, containing the *nikR* coding sequence cloned in frame within the NdeI/BamHI restriction sites	15

[a] IPTG, isopropyl-β-D-thiogalactopyranoside.

pected. The pattern of protection was evident on both DNA strands (Fig. 1B and C), although it appears better resolved on the noncoding strand. Analysis of nucleotide sequence of the protected regions revealed that short stretches of nucleotides (4 or 5 nucleotides) were directly contacted by *Hp*NikR, with 4 to 7 nucleotides separating each stretch (Fig. 1D). An offset of base protection of 2 or 3 nucleotides along the coding strand was observed, indicating that the binding of *Hp*NikR occurred on the same face of the DNA, in agreement with the characteristic protein-operator interaction of this family of regulators (33). As is evident from the nucleotide sequence shown in Fig. 1D, the regions containing the protected bases do not present any obvious extended palindromes; rather, a prevalence of A and T was observed. Intriguingly, the nucleotides protected

TABLE 2. Primers used for PCR amplification of the promoter regions and for primer extension reactions

Oligonucleotide name	Sequence (5′→3′)[a]
A3Fnew	ATTT*GGATCC*AGCGTCAAAGAATGTCTTGT
A3Rnew	TAAT*GAATTC*TTTCAAGTAGAATCACG
A3.11	TCC*CCCGGG*TATTACTTAATA
A3.12	TCC*CCCGGG*AAAAAAACTTAA
A3.13	TCC*CCCGGG*TTTTATTTTTAT
A3.14	TCC*CCCGGG*TAATAATTCGCA
A3.15	TCC*CCCGGG*AGGCGTTCGTTA
A3.16	TCC*CCCGGG*TAATAAAAATAA
A3.17	TCC*CCCGGG*TCTGCGAATTAT
A3.18	TCC*CCCGGG*TCATAAAAATTC
A3.19	TCC*CCCGGG*ATGATAAAATTC
A3.20	TCC*CCCGGG*TCTTAAAATTTT
A3.21	TCC*CCCGGG*AAGAATTTTTAT
A3.22	TCC*CCCGGG*TTATTAATCCCA
A3Z1	GTATCGATAAGCTTGATATC

[a] Bases in italics correspond to exogenous restriction sites.

within the two operators partially overlap the *Hp*NikR consensus sequence previously proposed by Delany et al. (15) (TATWATT-N_{11}-AATWATA) and recently revised by Stoof et al. (37) (TRWYA-N_{15}-TRWYA). A similar A-T base bias was reported for the hydroxyl radical pattern of protection of the *ureA* and *nixA* promoters (5), although the sequences and intersite spacing are different from the ones reported in this study.

Titration of *Hp*NikR binding to wild-type and mutant P_{fecA3} sequences. We assayed the binding to the *fecA3* promoter probe by electrophoretic mobility shift assay to determine the binding constant and to investigate how base substitutions within each operator would affect *Hp*NikR binding. The gel shift and binding curve relative to the wild-type promoter probe are shown in Fig. 2. The binding constant (K_{50}) was expressed as the relative amount of protein causing a 50% reduction of free probe, because the substitutions introduced within both operators compromised both the affinity of the protein for the DNA and the stability of the complex (see below). The derived K_{50} for the wild-type promoter is 3.5 nM, a value 10 times lower than the one previously reported for OP-I *fecA3* (20). This apparent discrepancy could be due to the different probes used. The DNA region utilized here contains both operators for *Hp*NikR, and this could account for the increased affinity. From the bases identified by hydroxyl radical footprinting, we designed six mutant promoter probes, where the short sequences contacted by *Hp*NikR were replaced one at a time with an SmaI site (Fig. 3A and B; see Materials and Methods and Table 2). Figure 3C to H shows the binding to the mutant promoters and the derived K_{50} values. We observed a strong reduction in binding caused by mutation of OP-I; in particular, the probe $P_{fecA3.15}$ (Fig. 3D) presented the highest reduction in affinity (almost 60 times lower), whereas $P_{fecA3.1}$ (Fig. 3C, 30 times lower) and $P_{fecA3.16}$ (Fig. 3E, 16 times lower) exhibited unstable binding as indicated by the diffused smearing across the lanes, in addition to a lower affinity. Similarly, the base substitutions within OP-II caused a reduction in affinity (between 13 and 22 times) and stability (Fig. 3F to H), although less intense. These observations suggest that both operators contribute to stable binding and affect the mobility shift, although the high-affinity sites (OP-I) are predominant. The different effects of the SmaI substitutions on the K_{50} correlate well with the positions of the base changes within the operators, suggesting an asymmetric structure of the protected bases within the operator, with a half-site (the one closer to +1, i.e., A3.15) being prevalent.

***In vivo* analysis of transcriptional *lacZ* fusions.** To evaluate how base substitutions at each subsite protected from hydroxyl radicals by *Hp*NikR *in vitro* would affect P_{fecA3} transcription *in vivo*, we measured the amount of transcripts produced by chromosomal wild-type and mutant P_{fecA3}::*lacZ* fusions. Therefore, fusions of mutant promoters to be introduced as an extra copy in the *vacA* locus of the *H. pylori* chromosome were generated (Table 1). The derived strains were grown to mid-log phase; then all cultures were split into two subcultures, one of which was treated with 1 mM $NiSO_4$ for 15 min. Afterwards, the growth was stopped, and the samples were collected and stored for RNA extraction to be used for primer extension analysis. The products of the retrotranscription reactions were separated on a denaturing gel. A representative set of reactions is shown in Fig. 4. The intensities of the bands corresponding to the +1 start site (see below) of three independent samples were quantified by ImageQuant, and for each construct the effect of nickel addition was expressed as the percentage of product relative to its untreated control, which was arbitrarily set to 100%. Different levels of RNA were observed depending upon the position of the SmaI site within the promoter. As expected, the wild-type promoter construct (Fig. 4, lanes 1 and 2) introduced in the *vacA* locus is regulated in response to nickel identically as in the native locus (12), and the nickel-dependent repression of P_{fecA3} occurred only for mutations mapping within OP-I (12). In particular, we were surprised by the transcript levels detected for the construct $P_{fecA3.1}$::*lacZ*, where the CCCGGG substitution maps in the middle of OP-I, as it showed a neat band, with intensity comparable to that of the wild-type construct (Fig. 4A, lane 3 versus lane 1). Moreover, addition of nickel caused a decrease in the amount of transcript with a residual level of 17% of the untreated sample (Fig. 4A, lanes 3 and 4). On the other hand, the construct $P_{fecA3.15}$::*lacZ* (the CCCGGG sequence is placed immediately downstream of +1) showed the most dramatic phenotype. A shift in the major 5′ end of RNA was observed (Fig. 4A, lanes 5 and 6), suggesting a possible faulty initiation of transcription and consequent repositioning of the start site, as bands appeared at positions −4 and +4 with respect to the original +1 (Fig. 4A, lanes 5 and 6). Upon nickel addition, the amount of RNA was nearly unchanged in comparison to that of the untreated sample (Fig. 4A, lanes 5 and 6), suggesting that the *Hp*NikR protein would no longer effectively bind to its operator *in vivo*. The construct $P_{fecA3.16}$::*lacZ*, with the CCCGGG sequence the farthest downstream from +1, also showed a shift of the start site with the likely +1 now mapping at −6 from the original site. The addition of nickel caused a 50% reduction of the level of RNA, indicative of a partially ineffective binding of *Hp*NikR (Fig. 4A, lanes 7 and 8). This construct also produced intense fast-migrating bands mapping at positions +22/23 with respect to the original +1 (see below). The construct $P_{fecA3.17}$::*lacZ*, with the CCCGGG substitution in part overlapping the −10 region, was not active, as expected (Fig. 4A, lanes 9 and 10). The constructs $P_{fecA3.19}$::*lacZ* and $P_{fecA3.21}$::*lacZ*,

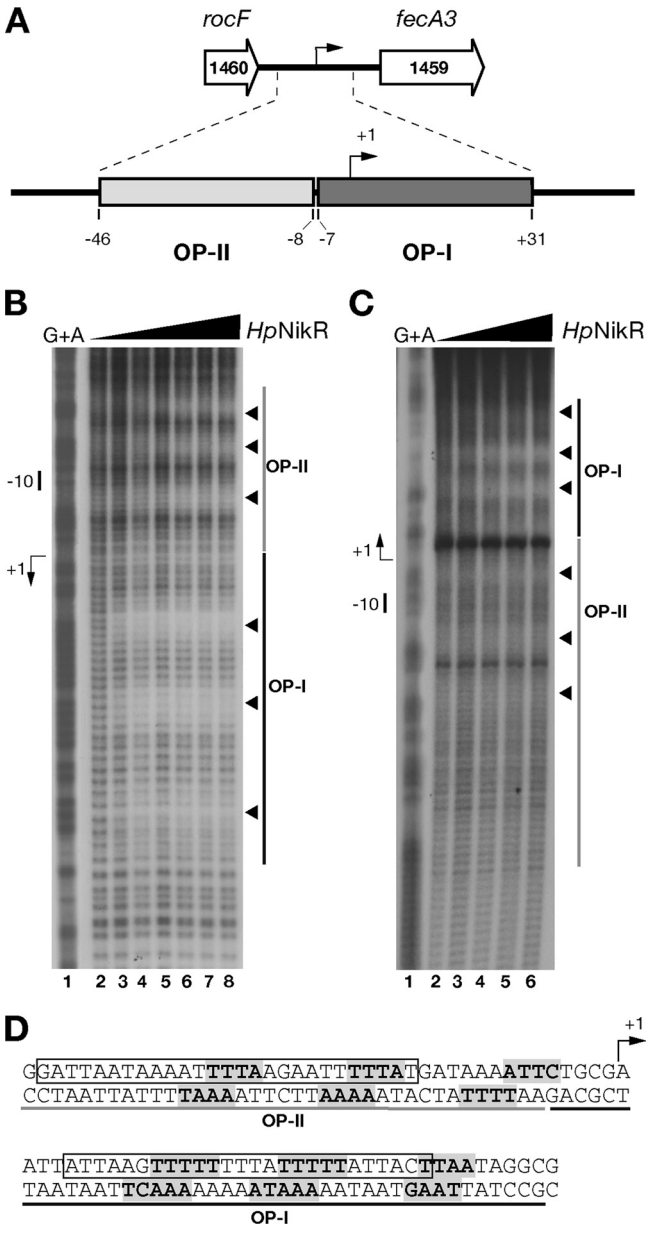

FIG. 1. Hydroxyl radical footprinting of Ni-*Hp*NikR on the P_{fecA3} region. (A) The *fecA3* gene of *H. pylori* G27 (HPG27_1459, nucleotides 1586410 to 1583885, minus strand) is separated by 352 nucleotides from the upstream gene *rocF* (HPG27_1460, nucleotides 1587730 to 1586762, minus strand). Two operator sites for *Hp*NikR were mapped by DNase I footprinting within this promoter: operator I (OP-I, dark gray), spanning nucleotides −7 to +31, and operator II (OP-II, light gray), spanning nucleotides −46 to −8. (B and C) DNA probes comprising the *fecA3* promoter were challenged with increasing concentrations of *Hp*NikR in a hydroxyl radical footprinting assay and separated on a denaturing sequencing gel. Approximately 20 fmol of 5′-end-labeled probes was incubated with increasing concentrations of protein (*Hp*NikR tetramer): 0 nM (lanes 1), 24.7 nM (lanes 2), 49 nM (lanes 3), 112.7 nM (lanes 4), 245 nM (lanes 5), 490 nM (lanes 6), 980 nM (lane 7), and 1,960 nM (lane 8). A G+A sequence reaction ladder of the each probe was run in parallel to map the bound bases with respect to the transcriptional start (+1) indicated by a bent arrow on the left side of each panel. The relative positions of OP-I and -II are represented by dark and light gray bars, respectively, and the short nucleotide segments protected by *Hp*NikR from hydroxyl radical cuts are shown by arrowheads on the right side. The separation gels were run at 54 W for a variable time (75 min to 3 h 15 min) to resolve the protected bases on each strand, and representative gels are shown for the noncoding (B) and coding (C) strands. Since the original cloning strategy placed the *Hp*NikR operators at about 50 bp in one case and at over 150 bp in the other with respect to the 5′-labeled ends, the base separation is better resolved along the noncoding strand than on the coding one. (D) Nucleotide sequences of the *fecA3* operators. The bases directly contacted by *Hp*NikR are shown in bold and shaded in gray. Three short stretches are protected along both OP-I and OP-II; the bent arrow shows the transcriptional start site. The sequences comprising OP-II and OP-I are underlined in gray and black, respectively. The sequence containing the consensus motif originally proposed by Delany et al. and the revised consensus proposed by Stoof et al. (15, 37) are boxed.

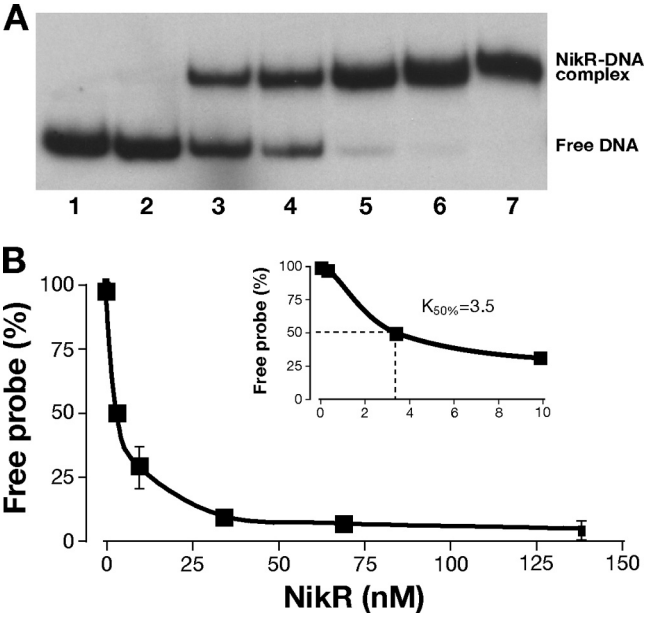

FIG. 2. Determination of Ni-*Hp*NikR K_{50} on P_{fecA3} wild type. (A) Electrophoretic mobility shifts of the wild-type promoter in the presence of increasing amounts of holo-*Hp*NikR and 200 ng of nonspecific competitor DNA. Lane 1, no protein added; lane 2, 0.34 nM; lane 3, 3.4 nM; lane 4, 9.8 nM, lane 5, 34 nM; lane 6, 68.6 nM; lane 7, 137.2 nM. Mobility shifts were quantified by ImageQuant analysis (Molecular Dynamics). (B) The K_{50} was extrapolated graphically by the binding curves. A K_{50} equal to 3.5 nM was derived from the binding curves obtained by plotting the percentage of free probe against increasing *Hp*NikR (inset). The error bars represent the standard deviations between the calculated K_{50}s of at least two independent experiments.

with the SmaI site farther upstream, maintained the nickel-dependent regulation, as the level of transcript dropped to approximately 10% and 20% of that of the untreated control in the presence of nickel, respectively (Fig. 4A, lanes 11 and 12 and lanes 13 and 14). The lack of effect of the base changes within OP-II is consistent with our previous study, where it was shown that OP-I is necessary and sufficient for the nickel-dependent repression (12). To confirm the physiological role of the base contacts established by *Hp*NikR within OP-I, we analyzed the levels of RNA transcripts of $P_{fecA3.1}$::*lacZ*, $P_{fecA3.15}$::*lacZ*, and $P_{fecA3.16}$::*lacZ* in the *nikR* deletion strain (Fig. 4B, lanes 1 to 6). As expected, the nickel-dependent

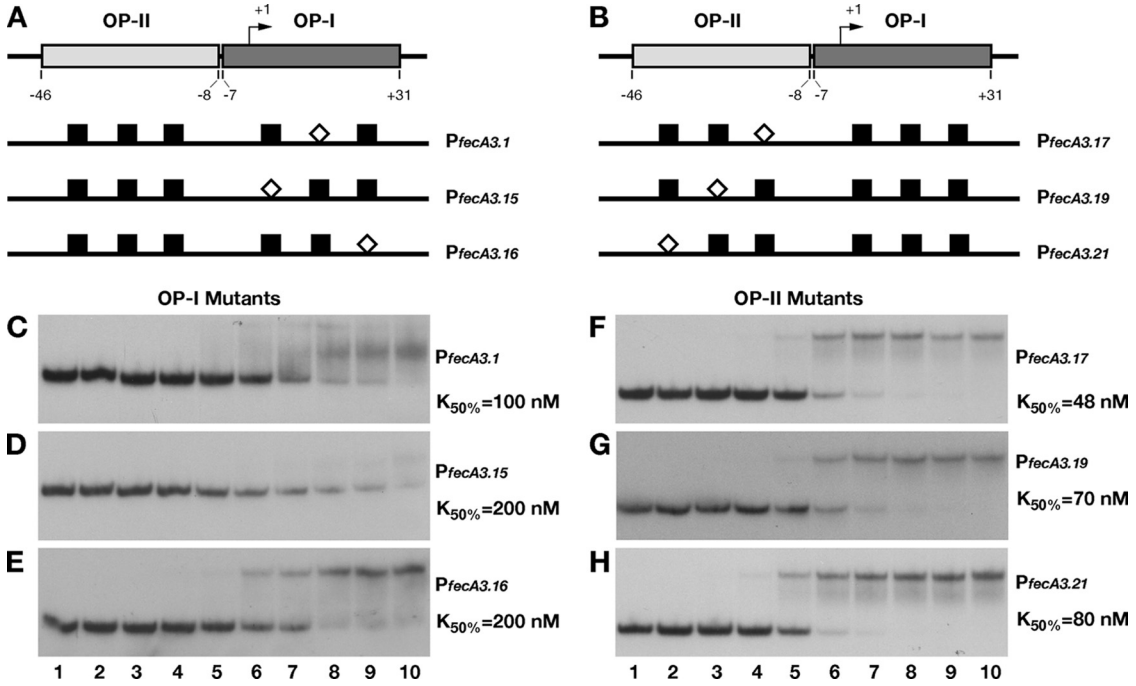

FIG. 3. DNA binding assays of mutant promoters. The introduction of a SmaI site in place of the bases protected by hydroxyl radical cuts on both operators strongly affected the affinity of *Hp*NikR for the whole promoter. A schematic representation of base substitutions within OP-I (A) and OP-II (B) is shown, with the white diamonds indicating the position of SmaI with respect to the wild-type sites (black boxes). Six mutant operator probes were generated ($P_{fecA3.1}$ [C], $P_{fecA3.15}$ [D], $P_{fecA3.16}$ [E], $P_{fecA3.17}$ [F], $P_{fecA3.19}$ [G], and $P_{fecA3.21}$ [H]) and analyzed by DNA retardation assay. *Hp*NikR was added at the following concentrations: 0 nM (no protein) (lanes 1), 0.34 nM (lanes 2), 3.4 nM (lanes 3), 9.8 nM (lanes 4), 34 nM (lanes 5), 68.6 nM (lanes 6), 137.2 nM (lanes 7), 274.4 nM (lanes 8), 343 nM (lanes 9), and 686 nM (lanes 10). The K_{50} was calculated as described for the wild-type construct (see legend to Fig. 2); in all cases, the standard deviation was less than 10% of the K_{50} value reported on the right site of each panel (C to H).

repression was lost for all constructs. Intriguingly, the shift of the major 5′ ends (constructs $P_{fecA3.15}$::*lacZ* and $P_{fecA3.16}$::*lacZ*, Fig. 4B, lanes 3 and 4 and lanes 5 and 6) and the intense bands at positions +22/23 (construct $P_{fecA3.16}$::*lacZ*, Fig. 4B, lanes 5 and 6) were also maintained in the *nikR* deletion strain. These data suggest that both features are *Hp*NikR independent and that the nucleotides substituted in these constructs might also be important for the accurate initiation of RNA transcription. Apparently, mutations at these nucleotide positions would produce a likely repositioning of the RNA polymerase synthesiz-

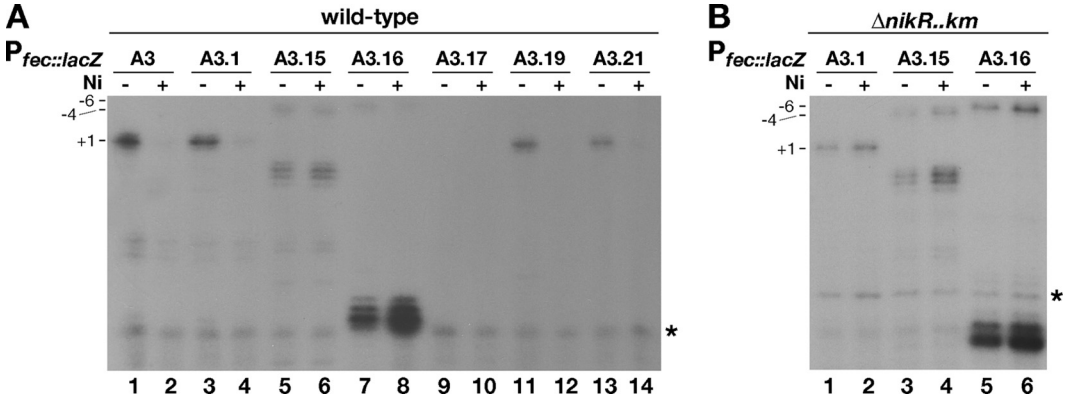

FIG. 4. *In vivo* transcription of the reporter constructs containing mutant promoters upon addition of nickel. Total RNA was extracted from cultures containing transcriptional fusions integrated in the *vacA* locus of *H. pylori* G27 wild-type (A) and *nikR* mutant (B) strains grown to exponential phase and treated for 15 min with 1 mM $NiSO_4$ (Ni). Positional marks are indicated. The $P_{fecA3.15}$::*lacZ* and $P_{fecA3.16}$::*lacZ* constructs have a shifted start site, whose position is numbered with respect to the original +1 site. The intensities of the bands were quantified by ImageQuant and expressed as the means of three independent experiments. The residual level of transcription upon addition of nickel is expressed as a percentage of the amount of transcript produced by each construct in the absence of nickel, with the values indicated: P_{fecA3}::*lacZ*, 10 ± 2; $P_{fecA3.1}$::*lacZ*, 17 ± 2.5; $P_{fecA3.15}$::*lacZ*, 90 ± 10; $P_{fecA3.16}$::*lacZ*, 52 ± 13; $P_{fecA3.17}$::*lacZ*, not detected; $P_{fecA3.19}$::*lacZ*, 10.5 ± 5; $P_{fecA3.21}$::*lacZ*, 19.5 ± 9.5. The asterisks on the right side of the gels represent the reference band.

ing RNA from new start sites. To test this hypothesis, we performed an *in vitro* transcription assay (not shown) using the plasmid constructs harboring wild-type and mutant promoters as templates with purified *E. coli* RNA polymerase, which was shown in the past to transcribe *H. pylori* genes accurately (3, 36). A similar pattern was observed, with shifted 5′ ends of RNA also produced by *in vitro* transcription experiments. Since the bands mapping *in vivo* at positions +4 ($P_{fecA3.15}$) and +22/23 ($P_{fecA3.16}$) were not produced in *in vitro* reactions and the complete analysis of the sequence did not suggest the presence of an alternative promoter, we interpreted these bands as possible *in vivo* degradation products.

In summary, our *in vivo* data showed that just one set of substitutions, $P_{fecA3.15}$::*lacZ*, completely abolished nickel-dependent repression. In accordance with the DNA mobility shift experiments, the nucleotide substitutions introduced in this half-site of OP-I were also critical for physiological regulation. With respect to the level of expression, we observed an amount of transcript produced by $P_{fecA3.1}$::*lacZ* comparable to that produced by the wild-type promoter. However, a smaller amount was detected for the promoters $P_{fecA3.15}$::*lacZ* and $P_{fecA3.16}$::*lacZ*. Consistent with a likely steric hindrance modality of repression occurring on this promoter, base substitutions along OP-I also affected the intrinsic strength of the promoter and consequently the amount of transcripts produced.

Hydroxyl radical footprinting of the mutant promoters. Notwithstanding the nucleotide substitutions, some of the mutant promoters still allowed the nickel-dependent repression of mutant P_{fecA3} *in vivo* (Fig. 4A), suggesting that somehow the *Hp*NikR protein would still effectively bind to the promoter *in vivo*. We therefore decided to determine the pattern of nucleotide protection from hydroxyl radicals along the mutant promoters upon *Hp*NikR binding. The binding reactions were conducted only for the noncoding strand of all constructs. The patterns of protection relative to the mutant constructs are shown in Fig. 5A to F; the sequence alignment of the nucleotides contacted by *Hp*NikR on all mutant operators is shown in Fig. 5G. In all cases, *Hp*NikR continued to bind to the promoters. However, considerable differences were observed in terms of base protection and binding affinity (compare Fig. 5A to F with Fig. 1B). First of all, the CCCGGG sequence seems to alter the contacts of *Hp*NikR within OP-II, which resulted in closer and partially overlapping OP-I. In detail, the construct $P_{fecA3.1}$, which allowed wild-type nickel repression (Fig. 4A), presented the same pattern of nucleotide protection within OP-I and a slightly modified profile within OP-II (compare Fig. 5A with Fig. 1B). In particular, *Hp*NikR still protects the set of bases in the middle of OP-I, where the CCCGGG site had been introduced, indicating that at these positions *Hp*NikR does not recognize the sequence. Accordingly, this pattern of binding correlates with the *Hp*NikR-dependent repression maintained *in vivo* (Fig. 4A). The construct $P_{fecA3.15}$, which *in vivo* abolished nickel repression (Fig. 4A), shows four protected DNA segments on the whole promoter arranged in between the two original operators, and the overall affinity of the protein for this promoter is almost 4.5 times lower than that for the wild type (compare Fig. 1B with Fig. 5B). In particular, within the original OP-I, the nucleotide positions now occupied by the CCCGGG sequence were the only subsite protected from the hydroxyl radicals, but *in vivo* this interaction must not be effective, as the regulation is lost. The construct $P_{fecA3.16}$ also showed a different pattern of binding, resulting in four stretches of nucleotides protected across the two original operators (Fig. 5C). However, the binding of *Hp*NikR *in vivo* may not be very tight, since a 50% "leaky" level of transcript was observed in the presence of nickel (Fig. 4). The constructs $P_{fecA3.17}$, $P_{fecA3.19}$, and $P_{fecA3.21}$ maintained mostly the original pattern of protection within OP-I (Fig. 5D to F), which is consistent with the *in vivo* transcription data (Fig. 4), leaving $P_{fecA3.17}$ aside because of the inactivated −10 box. On the other hand, the profile of protected bases within OP-II is modified (Fig. 5G). Interestingly, the construct $P_{fecA3.19}$ showed a strong reduction in affinity and just two segments of protection within OP-I (Fig. 5E). However, these interactions seem to be sufficient to allow a productive binding and nickel-dependent repression *in vivo* (Fig. 4, lanes 11 and 12).

In summary, all mutations on both operators modify the wild-type pattern of protected bases along the OP-II sequence, indirectly confirming the cooperative binding of *Hp*NikR on the two operators and also suggesting a reorganization of the interactions between the protein and its target DNA. The modified pattern of protection from hydroxyl radical cuts suggests that *Hp*NikR may recognize bases within the consensus sequences and subsequently make contacts with neighboring nucleotides, likely depending upon structural DNA motifs.

Hydroxyl radical footprinting of the $P_{nikR\text{-}exbB}$ region. To verify whether the sequence features identified along the *fecA3* promoter are shared by other *Hp*NikR-regulated genes, we carried out hydroxyl radical footprinting on the *nikR-exbB* intergenic region, containing the respective *nikR* and *exbB* promoters, where low-affinity *Hp*NikR operators (approximately 40 bp in both cases) were previously mapped by DNase I footprinting (15). As shown in Fig. 6, four subsites protected from hydroxyl radical cuts were identified on P_{nikR}, whereas three subsites were present on P_{exbB}. Again, the bases protected presented a prevalence of A and T, and the sites of protection were 2 or 3 bases offset between the two strands, confirming that the binding of *Hp*NikR occurred on the same face of the DNA. However, no obvious conservation of sequence and position of protected sites within the operators was observed when the three promoters, P_{fecA3}, P_{nikR}, and P_{exbB}, were compared, suggesting that *Hp*NikR must have a high degree of tolerance in terms of bases protected. Moreover, the affinity of *Hp*NikR for a specific promoter appeared not to lay down the number of sites of interactions since both P_{nikR} and P_{exbB} have two low-affinity operators (15, 20) but showed four and three protection sites, respectively.

DISCUSSION

*Hp*NikR-regulated promoters do not share well-conserved operators (20). Here, we present evidence on the nucleotides protected on the *fecA3*, *exbB*, and *nikR* promoters and the effect that introducing sequence-specific mutations has on the *in vivo* interaction of *Hp*NikR with P_{fecA3}. Our results indicate that *Hp*NikR protects a different number of subsites within its operators and that there is no correlation between how many subsites are protected from hydroxyl radical cleavages and the affinity that *Hp*NikR has for that particular operator. As shown in Fig. 6, the low-affinity operators of P_{exbB} and P_{nikR}, which

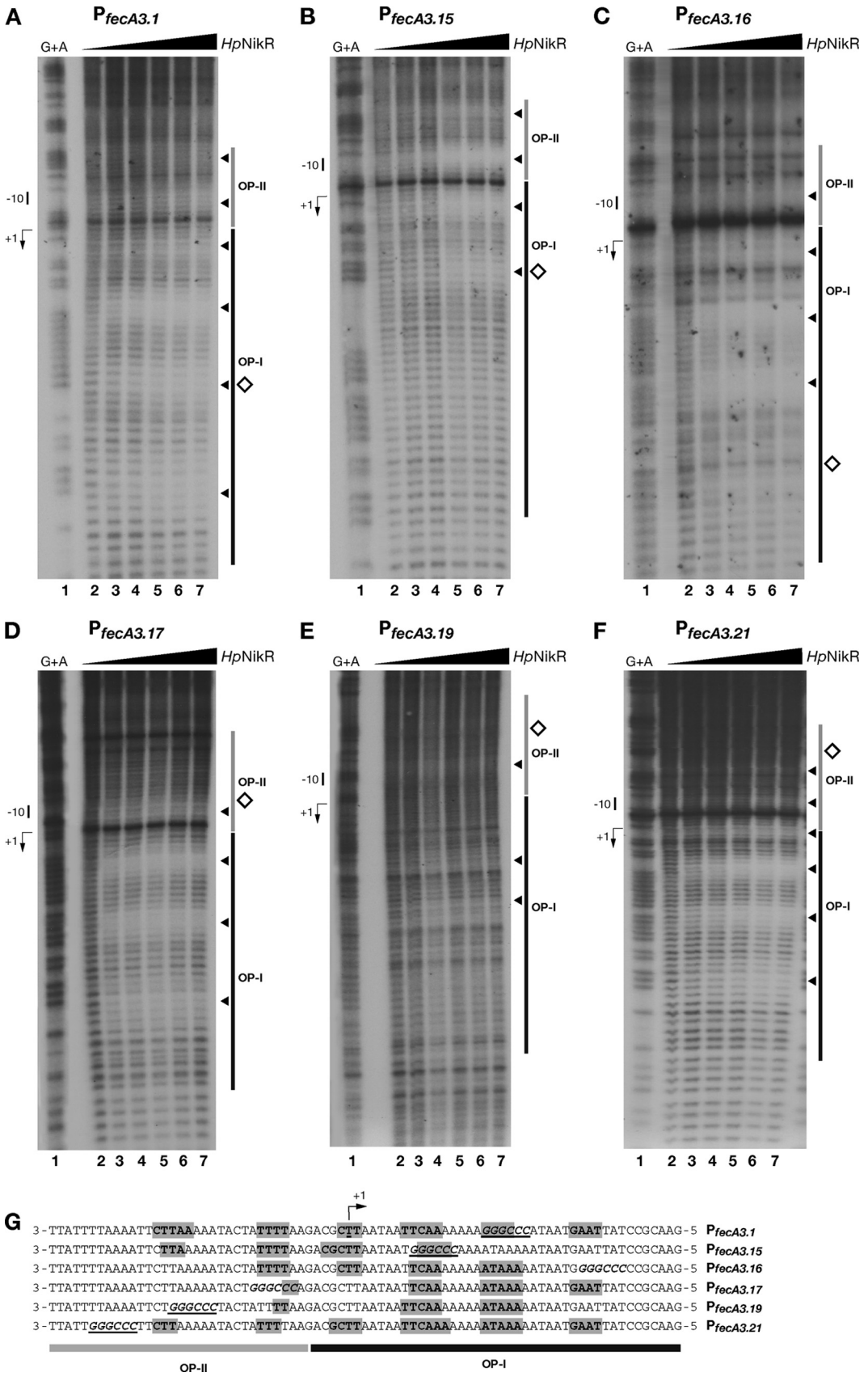
A
P fecA3.1
G+A
HpNikR
-10
+1
OP-II
OP-I
1 2 3 4 5 6 7
B
P fecA3.15
G+A
HpNikR
-10
+1
OP-II
OP-I
1 2 3 4 5 6 7
C
P fecA3.16
G+A
HpNikR
-10
+1
OP-II
OP-I
1 2 3 4 5 6 7
D
P fecA3.17
G+A
HpNikR
-10
+1
OP-II
OP-I
1 2 3 4 5 6 7
E
P fecA3.19
G+A
HpNikR
-10
+1
OP-II
OP-I
1 2 3 4 5 6 7
F
P fecA3.21
G+A
HpNikR
-10
+1
OP-II
OP-I
1 2 3 4 5 6 7
G
+1
3-TTATTTTAAAATTCTTAAAAATACTATTTTAAGACGCTTAATAATTCAAAAAAAGGGCCCATAATGAATTATCCGCAAG-5 PfecA3.1
3-TTATTTTAAAATTCTTAAAAATACTATTTTAAGACGCTTAATAATGGGCCCAAAATAAAAATAATGAATTATCCGCAAG-5 PfecA3.15
3-TTATTTTAAAATTCTTAAAAATACTATTTTAAGACGCTTAATAATTCAAAAAAAATAAAAATAATGGGCCCCCGCAAG-5 PfecA3.16
3-TTATTTTAAAATTCTTAAAAATACTGGGCCCAGACGCTTAATAATTCAAAAAAAATAAAAATAATGAATTATCCGCAAG-5 PfecA3.17
3-TTATTTTAAAATTCTGGGCCCTACTATTTTAAGACGCTTAATAATTCAAAAAAAATAAAAATAATGAATTATCCGCAAG-5 PfecA3.19
3-TTATTGGGCCCTTCTTAAAAATACTATTTTAAGACGCTTAATAATTCAAAAAAAATAAAAATAATGAATTATCCGCAAG-5 PfecA3.21
OP-II
OP-I

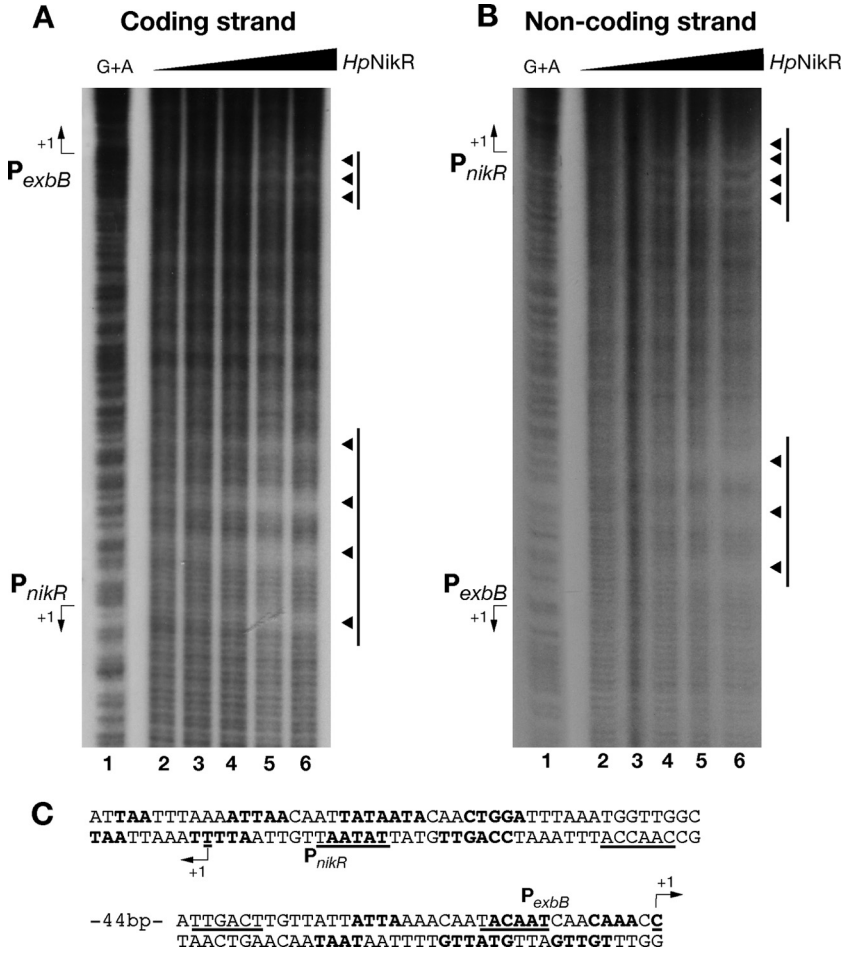

FIG. 6. Hydroxyl radical footprinting of Ni-*Hp*NikR on the $P_{nikR\text{-}exbB}$ divergent promoter locus. (A and B) Profile of base protection of the coding (A) and noncoding (B) strands of the *nikR-exbB* promoter region with increasing amounts of holo-*Hp*NikR. Lanes 1, G+A ladder; lanes 2, no protein; lanes 3, 0.122 μM; lanes 4, 0.245 μM; lanes 5, 0.490 μM; lanes 6, 1.47 μM. Bars and arrowheads to the right of the panels represent the *Hp*NikR operators and protection sites, respectively. (C) Sequences of the promoters. Promoter features (+1, −10, and −35) are underlined, and the protected bases are in bold. The operators for *Hp*NikR on P_{nikR} and P_{exbB} span nucleotides −27 to +10 and −37 to +1, respectively, with respect to each promoter transcriptional start site.

*Hp*NikR binds to rather weakly, have three and four subsites, respectively. Conversely, *Hp*NikR protects three subsites within both the high-and low-affinity operators of P_{fecA3}. It also is quite evident that the sequence and length of each subsite vary depending on the promoter being studied (Fig. 1D and 6C).

All the subsites on P_{fecA3} identified here severely reduced *Hp*NikR binding *in vitro* when mutated (Fig. 2 and 3). However, only two operator mutants affected *fecA3* expression *in vivo* (Fig. 4), that is, the promoter transcriptional fusions with mutations at the farther ends of OP-I, completely or in part, failed to repress *fecA3* in the presence of nickel. The available data about the binding of native and recombinant *Hp*NikR to the promoter regions of *ureA*, *exbB*, and *nikR* show no differences in the patterns of interaction (1, 15, 20, 45). This suggests that the three additional residues, remaining on the recombinant NikR used in this study, may not interfere with its binding activity and argue against the discrepancy between our *in vivo*

FIG. 5. Bases contacted by Ni-*Hp*NikR within P_{fecA3} mutant promoters. (A to F) Pattern of protection from hydroxyl radicals for the probes $P_{fecA3.1}$ (A), $P_{fecA3.15}$ (B), $P_{fecA3.16}$ (C), $P_{fecA3.17}$ (D), $P_{fecA3.19}$ (E), and $P_{fecA3.21}$ (F) by increasing concentrations of protein, expressed per *Hp*NikR tetramer, corresponding to 0 nM (lanes 2), 24.7 nM (lanes 3), 49 nM (lanes 4), 112.7 nM (lanes 5), 245 nM (lanes 6), and 490 nM (lanes 7). A G+A sequence reaction ladder (lanes 1) of the promoter probes was run in parallel to map the bound bases with respect to the transcriptional start (+1) indicated by a bent arrow on the left side of each representative gel. The dark and light gray bars on the right side of each gel show the original positions of the operators, whereas the white diamonds represent the position of the SmaI site and the black arrowheads indicate the bases protected at increasing protein concentrations. (G) Alignment of the noncoding strands of all six mutant operators: the bases protected are in bold and shaded in gray, and the SmaI sequence is in bold italics and underlined. Some of the nucleotide contacts are conserved in spite of the base substitutions.

and *in vitro* data. The comparative analysis of our *in vivo* and *in vitro* data therefore allows us to conclude that all nucleotide interactions occurring *in vitro* strongly decrease binding but may have a negligible effect *in vivo*, suggesting that the native DNA conformation may play a role in the promoter recognition and binding, as is common in many bacterial regulatory interactions (6, 28). It is worth noting that the conformation of the promoter may be distorted and bent upon correct *Hp*NikR binding to one half of the operator, so as to favor cooperative binding to the second half-site, and that the base substitution utilized in this study (CCCGGG) may alter the overall DNA conformation, as it is known that GC-rich DNA tracts widen the double-helix minor groove (30) and therefore deform the natural/native DNA conformation. In this respect, the patterns of protection shown by mutant promoters (Fig. 5G) indicate that *Hp*NikR *in vitro* may maintain its contacts at some of the original positions of interaction, regardless of the nucleotide sequence, but that the remaining subsites may be either missing or rearranged along the promoter. Cases in point are the nucleotide interactions displayed on the constructs $P_{fecA3.15}$ and $P_{fecA3.16}$ (Fig. 5). *Hp*NikR still binds the nucleotide positions mutated on $P_{fecA3.15}$, but this is not sufficient to attach the regulator to the operator properly (loss of nickel repression, Fig. 4A, lanes 5 and 6), suggesting that the CCCGGG sequence may have altered the double-helix conformation. On the other hand, *Hp*NikR binds to $P_{fecA3.16}$ (Fig. 5C and G) in a partially permissive way that allows maintenance of about 50% nickel-dependent *Hp*NikR repression (Fig. 4A, lanes 7 and 8). In this second instance, however, the nucleotide positions, now occupied by CCCGGG, no longer are sites of protection and the two original subsites within OP-I are sufficient for the regulative function.

An *Hp*NikR asymmetric mode of interaction with DNA was first noted by Delany et al. (15). These authors reported how base mutations along the operator of the *Hp*NikR-activated promoter *ureA* impaired binding in a DNase I footprinting assay, with mutations in one half-site being more effective. Recently, Dosanjh et al. (20) showed that an engineered perfectly symmetric *ureA* operator had a lower affinity than did the wild-type one and that base substitutions in the two half-sites differently contribute to tight binding. Our *in vivo* data strongly support these previous reports, based on *in vitro* observations, and suggest that one half-site may serve to anchor *Hp*NikR specifically to the operator and allow the rest of the tetramer to adapt to the promoter. It is also possible that the physical form of DNA *in vivo* may play a role (30) in the binding of the regulator. In this respect, it has been shown how the residues on the *Hp*NikR N-terminal arm make specific contact on some promoters (5).

The *E. coli* NikR homolog is a repressor, which accomplishes its role by recognizing with high affinity a symmetric dyad, 5′-GTAGTA-N_{16}-TCATAC-3′, embedded in its unique target operator (9). The structure of the complex *Ec*NikR-*nik* operator was resolved (35), providing details about the intrinsic structural changes triggered by DNA binding, which are possibly shared by all NikR homologs. First, the holo-NikR tetramer displays high interdomain flexibility, orienting all the RHH domains toward the DNA major groove of the target operator. Second, polar interactions take place between protein and operator nucleotides and the DNA phosphate backbone. Third, unspecific electrostatic interactions occur between the NikR metal binding domain and the phosphate backbone of the operator minor groove, in addition to polar interactions at the center of the operator. It would be interesting to have structural data for the holo-*Hp*NikR/DNA complex to understand the molecular mechanisms guiding the interactions between *Hp*NikR surface residues and exposed nucleotides. Given the intrinsic complexity of *Hp*NikR and its abilities to discriminate between high- and low-affinity operators; to display a pH-dependent, nickel-insensitive DNA binding activity; and to establish a multiplicity of sequence contacts along its regulatory targets, it is reasonable to anticipate that *Hp*NikR may have a large repertoire of possible interactions with DNA and that, therefore, more than one solved regulator/operator complex may be necessary to provide a detailed picture of binding. The first crystal structure of holo-*Hp*NikR has very recently become available (42). It revealed that *Hp*NikR displays two discrete geometries of nickel coordination within the native tetramer, suggesting that the intrinsic asymmetric arrangement of the physiological effector may be reflected by the DNA binding activity of the transcriptional regulator.

In conclusion, the data presented here support an asymmetric mode of recognition *in vivo* of a high-affinity target operator (P_{fecA3} OP-I) by the native *Hp*NikR. This model is consistent with the lack of extended and conserved symmetry elements between half-sites in all the operators so far experimentally characterized and suggests that *Hp*NikR might have evolved different mechanisms for binding. In a broader context, the experiments presented point to an operator-specific pattern of interactions. Although the proposed consensus motif for *Hp*NikR would be a valuable predictive tool, likely containing the elements allowing the initial recognition of a target operator, the comparison among base contacts identified in this study and in the work of Benanti and Chivers (5) shows that there are no obvious sequence hallmarks for *Hp*NikR contacts and that the specificities of *Hp*NikR-protected nucleotides are not conserved among the operators analyzed. The high degree of sequence degeneracy may be essential to *Hp*NikR to fulfill its multifunction regulatory role.

ACKNOWLEDGMENTS

This work was funded by grants A.98.726 (Rientro dei Cervelli 2008-2010-MiUR) to S.R. and RFO 2008 to V.S.

We thank G. Corsi for artwork.

REFERENCES

1. **Abraham, L. O., Y. Li, and D. B. Zamble.** 2006. The metal- and DNA-binding activities of *Helicobacter pylori* NikR. J. Inorg. Biochem. **100:**1005–1014.
2. **Bahlawane, C., et al.** 2010. Structural and mechanistic insights into *Helicobacter pylori* NikR activation. Nucleic Acids Res. **38:**3106–3118.
3. **Beier, D., G. Spohn, R. Rappuoli, and V. Scarlato.** 1998. Functional analysis of the *Helicobacter pylori* principal sigma subunit of RNA polymerase reveals that the spacer region is important for efficient transcription. Mol. Microbiol. **30:**121–134.
4. **Benanti, E. L., and P. T. Chivers.** 2009. An intact urease assembly pathway is required to compete with NikR for nickel ions in *Helicobacter pylori*. J. Bacteriol. **191:**2405–2408.
5. **Benanti, E. L., and P. T. Chivers.** 2007. The N-terminal arm of the *Helicobacter pylori* Ni2+-dependent transcription factor NikR is required for specific DNA binding. J. Biol. Chem. **282:**20365–20375.
6. **Browning, D. F., and S. J. Busby.** 2004. The regulation of bacterial transcription initiation. Nat. Rev. Microbiol. **2:**57–65.
7. **Bury-Mone, S., et al.** 2004. Responsiveness to acidity via metal ion regulators mediates virulence in the gastric pathogen *Helicobacter pylori*. Mol. Microbiol. **53:**623–638.

8. **Chivers, P. T., and R. T. Sauer.** 1999. NikR is a ribbon-helix-helix DNA-binding protein. Protein Sci. **8:**2494–2500.
9. **Chivers, P. T., and R. T. Sauer.** 2000. Regulation of high affinity nickel uptake in bacteria. Ni2+-dependent interaction of NikR with wild-type and mutant operator sites. J. Biol. Chem. **275:**19735–19741.
10. **Contreras, M., J. M. Thiberge, M. A. Mandrand-Berthelot, and A. Labigne.** 2003. Characterization of the roles of NikR, a nickel-responsive pleiotropic autoregulator of *Helicobacter pylori*. Mol. Microbiol. **49:**947–963.
11. **Costa, M., et al.** 2001. Plasmid transcriptional repressor CopG oligomerises to render helical superstructures unbound and in complexes with oligonucleotides. J. Mol. Biol. **310:**403–417.
12. **Danielli, A., et al.** 2009. Growth phase and metal-dependent transcriptional regulation of the fecA genes in *Helicobacter pylori*. J. Bacteriol. **191:**3717–3725.
13. **Danielli, A., and V. Scarlato.** 2010. Regulatory circuits in *Helicobacter pylori*: network motifs and regulators involved in metal-dependent responses. FEMS Microbiol. Rev. **34:**738–752.
14. **Davis, G. S., E. L. Flannery, and H. L. Mobley.** 2006. *Helicobacter pylori* HP1512 is a nickel-responsive NikR-regulated outer membrane protein. Infect. Immun. **74:**6811–6820.
15. **Delany, I., et al.** 2005. In vitro analysis of protein-operator interactions of the NikR and fur metal-responsive regulators of coregulated genes in *Helicobacter pylori*. J. Bacteriol. **187:**7703–7715.
16. **Delany, I., G. Spohn, R. Rappuoli, and V. Scarlato.** 2002. Growth phase-dependent regulation of target gene promoters for binding of the essential orphan response regulator HP1043 of *Helicobacter pylori*. J. Bacteriol. **184:**4800–4810.
17. **De Pina, K., V. Desjardin, M. A. Mandrand-Berthelot, G. Giordano, and L. F. Wu.** 1999. Isolation and characterization of the nikR gene encoding a nickel-responsive regulator in *Escherichia coli*. J. Bacteriol. **181:**670–674.
18. **Dian, C., et al.** 2006. Structural basis of the nickel response in *Helicobacter pylori*: crystal structures of HpNikR in apo and nickel-bound states. J. Mol. Biol. **361:**715–730.
19. **Dosanjh, N. S., N. A. Hammerbacher, and S. L. Michel.** 2007. Characterization of the *Helicobacter pylori* NikR-P(ureA) DNA interaction: metal ion requirements and sequence specificity. Biochemistry **46:**2520–2529.
20. **Dosanjh, N. S., A. L. West, and S. L. Michel.** 2009. *Helicobacter pylori* NikR's interaction with DNA: a two-tiered mode of recognition. Biochemistry **48:**527–536.
21. **Ernst, F. D., et al.** 2005. The nickel-responsive regulator NikR controls activation and repression of gene transcription in *Helicobacter pylori*. Infect. Immun. **73:**7252–7258.
22. **Ernst, F. D., et al.** 2006. NikR mediates nickel-responsive transcriptional repression of the *Helicobacter pylori* outer membrane proteins FecA3 (HP1400) and FrpB4 (HP1512). Infect. Immun. **74:**6821–6828.
23. **Hanahan, D.** 1983. Studies on transformation of *Escherichia coli* with plasmids. J. Mol. Biol. **166:**557–580.
24. **Li, Y., and D. Zamble.** 2009. The pH-responsive DNA-binding activity of *Helicobacter pylori* NikR. Biochemistry **48:**2486–2496.
25. **Liu, S. T., and G. F. Hong.** 1998. Three-minute G + A specific reaction for DNA sequencing. Anal. Biochem. **255:**158–159.
26. **Ni, L., et al.** 2009. The *Staphylococcus aureus* pSK41 plasmid-encoded ArtA protein is a master regulator of plasmid transmission genes and contains a RHH motif used in alternate DNA-binding modes. Nucleic Acids Res. **37:**6970–6983.
27. **Overgaard, M., J. Borch, and K. Gerdes.** 2009. RelB and RelE of *Escherichia coli* form a tight complex that represses transcription via the ribbon-helix-helix motif in RelB. J. Mol. Biol. **394:**183–196.
28. **Perez-Martin, J., and V. de Lorenzo.** 1997. Clues and consequences of DNA bending in transcription. Annu. Rev. Microbiol. **51:**593–628.
29. **Pflock, M., S. Kennard, I. Delany, V. Scarlato, and D. Beier.** 2005. Acid-induced activation of the urease promoters is mediated directly by the ArsRS two-component system of *Helicobacter pylori*. Infect. Immun. **73:**6437–6445.
30. **Rohs, R., W. S. M. A. Sosinsky, P. Liu, R. S. Mann, and B. Honig.** 2009. The role of DNA shape in protein-DNA recognition. Nature **461:**1248–1254.
31. **Sachs, G., D. L. Weeks, K. Melchers, and D. R. Scott.** 2003. The gastric biology of *Helicobacter pylori*. Annu. Rev. Physiol. **65:**349–369.
32. **Sambrook, J., E. F. Fritsch, and T. Maniatis.** 1989. Molecular cloning: a laboratory manual, 2nd ed. Cold Spring Harbor Laboratory Press, Cold Spring Harbor, NY.
33. **Schreiter, E. R., and C. L. Drennan.** 2007. Ribbon-helix-helix transcription factors: variations on a theme. Nat. Rev. Microbiol. **5:**710–720.
34. **Schreiter, E. R., et al.** 2003. Crystal structure of the nickel-responsive transcription factor NikR. Nat. Struct. Biol. **10:**794–799.
35. **Schreiter, E. R., S. C. Wang, D. B. Zamble, and C. L. Drennan.** 2006. NikR-operator complex structure and the mechanism of repressor activation by metal ions. Proc. Natl. Acad. Sci. U. S. A. **103:**13676–13681.
36. **Spohn, G., D. Beier, R. Rappuoli, and V. Scarlato.** 1997. Transcriptional analysis of the divergent cagAB genes encoded by the pathogenicity island of *Helicobacter pylori*. Mol. Microbiol. **26:**361–372.
37. **Stoof, J., E. J. Kuipers, and A. H. van Vliet.** 2010. Characterization of NikR-responsive promoters of urease and metal transport genes of *Helicobacter mustelae*. Biometals **23:**145–159.
38. **Studier, F. W., and B. A. Moffatt.** 1986. Use of bacteriophage T7 RNA polymerase to direct selective high-level expression of cloned genes. J. Mol. Biol. **189:**113–130.
39. **van Vliet, A. H., F. D. Ernst, and J. G. Kusters.** 2004. NikR-mediated regulation of *Helicobacter pylori* acid adaptation. Trends Microbiol. **12:**489–494.
40. **van Vliet, A. H., et al.** 2002. NikR mediates nickel-responsive transcriptional induction of urease expression in *Helicobacter pylori*. Infect. Immun. **70:**2846–2852.
41. **Wang, Y., and D. E. Taylor.** 1990. Chloramphenicol resistance in *Campylobacter coli*: nucleotide sequence, expression, and cloning vector construction. Gene **94:**23–28.
42. **West, A. L., et al.** 2010. Holo-Ni(II) *Hp*NikR is an asymmetric tetramer containing two different nickel-binding sites. J. Am. Chem. Soc. **132:**14447–14456.
43. **Wolfram, L., E. Haas, and P. Bauerfeind.** 2006. Nickel represses the synthesis of the nickel permease NixA of *Helicobacter pylori*. J. Bacteriol. **188:**1245–1250.
44. **Xiang, Z., et al.** 1995. Analysis of expression of CagA and VacA virulence factors in 43 strains of *Helicobacter pylori* reveals that clinical isolates can be divided into two major types and that CagA is not necessary for expression of the vacuolating cytotoxin. Infect. Immun. **63:**94–98.
45. **Zambelli, B., et al.** 2008. High-affinity Ni2+ binding selectively promotes binding of *Helicobacter pylori* NikR to its target urease promoter. J. Mol. Biol. **383:**1129–1143.
46. **Zaychikov, E., P. Schickor, L. Denissova, and H. Heumann.** 2001. Hydroxyl radical footprinting. Methods Mol. Biol. **148:**49–61.